DTU Library

Hierarchical Frequency Control of Hybrid Power Plants Using Frequency Response Observer

Long, Qian; Das, Kaushik; Sørensen, Poul

Link back to DTU Orbit

Hierarchical Frequency Control of Hybrid Power Plants Using Frequency Response Observer

Qian Long, *Member, IEEE,* Kaushik Das, *Senior Member, IEEE,* and Poul Sørensen, *Fellow, IEEE*

Abstract—With frequency stability being challenged in modern power systems, transmission system operators have been designing new mitigation measures, such as fast frequency response (FFR), to maintain operation security of power systems. To accommodate technical requirements of new frequency control services (FCSs), the corresponding control should be implemented at asset controllers to enable fast responses. However, control counteraction can arise between plant controllers and asset controllers during the provision of FCSs. In this paper, a novel hierarchical frequency control approach is proposed to allow hybrid power plants (HPPs) to provide three types of FCSs, namely FFR, frequency containment response (FCR) and frequency restoration response (FRR). To solve control counteraction issue, an innovative frequency response observer (FROB) is proposed. The FROB at plant controllers and the hybrid power plant controller (HPPC) accurately estimates frequency response initiated by asset controllers, and the obtained estimation is used for control compensation at plant controllers and the HPPC to avoid control counteraction. Design guidelines and robustness analysis of the FROB are then discussed. Case studies are implemented in a power system dynamic model in MATLAB/Simulink, and the results show that the proposed frequency control approach enables coordinated operation of multiple technology power plants, with robust performance achieved when there are system uncertainties in HPPs.

Index Terms—hierarchical frequency control, hybrid power plants, fast frequency response, disturbance observers, frequency response observers.

I. INTRODUCTION

AS frequency stability has been challenged by the increasing share of inverter-based resources in modern power systems, the requirement for frequency control (FC) becomes demanding, posing challenges for the existing FC methods for power plants [1]. Utility-scale hybrid power plants (HPPs) have received global attention due to enhanced controllability and efficient utilization of electrical infrastructure [2]–[4]. For the time being, there is a lack of consensus in academic literature on the definition of HPPs. For the sake of our work, HPPs are defined to be exclusively utility-scale grid-connected systems including multiple types of generation resources. How to design FC methods for HPPs to fulfil the latest requirements need to be further investigated. Besides, the complexity of FC design for HPPs is increased compared to single-technology power plants since there are heterogeneous assets and controllers in an HPP that need to be coordinated [5]. However, there is little literature addressing FC of HPPs [6], [7].

Hierarchical FC for single-technology power plants, which involves one plant controller and multiple asset controllers, has been well established. A conventional approach is to
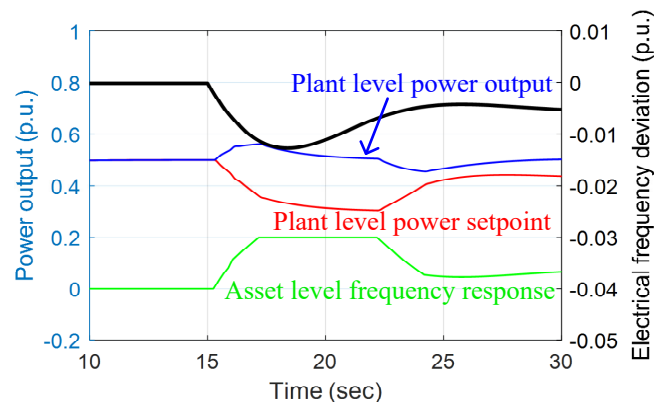

Fig. 1: An example of control counteraction during an under-frequency event.

introduce auxiliary FC loop for active power control at the plant controller, which generates time-varying active power setpoints for asset controllers when FC is activated [8]–[11]. While this approach is easy to implement in the power plant controller and enables power plants to provide frequency control services (FCSs) such as FCR and FRR, factors such as communication delay and limited control bandwidth could be the bottleneck for the plant controller to provide fast FCSs required by future power systems with low inertia. This approach from literature might lead to frequency responses slower than the requirements. To date, fast FC has been mostly implemented at asset controllers for wind turbines (WTs), photovoltaics (PVs) and energy storage (ESs) [12]–[18]. Nevertheless, very few works on power plant control adapt to these state-of-the-art fast FC design. It is worth pointing out that, without any coordination strategy, the plant controller will counteract against asset controllers, at which frequency response is activated, during a frequency event. Fig. 1 shows an example of such control counteraction. Therefore, a new hierarchical FC approach that supports fast FC at asset controllers and coordinates between the plant controller and asset controllers during the period of FCS provision is in need.

The main challenge of the coordination arises from frequency response being an unknown control action, as seen by the hybrid power plant controller (HPPC) and plant controllers, from asset controllers. A possible way of addressing control counteraction is to estimate the total frequency response and then to add as the compensation term to the HPPC and plant controllers. However, uncertainties existing in HPPs, such as unknown parameters, control malfunction and communication delay, bring extra challenges into accurate estimation

of frequency response. Besides, considering the HPPC as an extra control level on top of wind power plant controller (WPPC), solar power plant controller (SPPC) and energy storage system controller (ESSC), the design of the coordination strategy across the whole control hierarchy becomes even more complicated [19]. This leads to one of the innovations in the paper, which is to develop a robust observer that can accurately estimate the total frequency response activated at asset controllers given system uncertainties, for the purpose of avoiding counteraction across control hierarchy.

Disturbance observers (DOBs) algorithms for estimating system uncertainties and disturbances, have been used extensively in various power-related industrial applications. Time-domain DOBs, such as extended-state observer, have been utilized in the field of load frequency control to estimate total disturbance from loads and renewable generation [20], [21]. In [22], similar DOB techniques have been applied to the charging and discharging control of a flywheel ESS in order to estimate model uncertainties and external disturbances. Another category of DOBs, that is, frequency-domain DOBs, have been proposed and adopted in applications like load frequency control [23], converter control [24] and PV generation [25]. The above-mentioned DOBs help generate a robust control system that achieves good performance in disturbance rejection and handles system uncertainties at the same time. This paper focuses on frequency-domain DOBs originally proposed in [26] due to its simple and straightforward nature. However, it should be emphasized that frequency-domain DOBs can not be directly applied as a solution to the above-mentioned control counteraction issue. It is because the design purpose of frequency-domain DOBs is to reject external disturbance, while frequency response from asset controllers is supposed to be accepted rather than rejected by plant controllers and the HPPC. Therefore, a new observer called frequency response observer (FROB) is developed following the idea of frequency-domain DOBs, such that the total frequency response from asset controllers is estimated as "the disturbance" and the closed-loop characteristic of FROB accepts this disturbance. The modification also leads to the need to establish new design guidelines.

As described above, the existing literature only focuses on either frequency control implemented at a centralized power plant controller or fast frequency control implemented at asset controllers. However, in order for renewable power plants to provide proper frequency control services that meet increasingly-strict technical requirements, the state-of-the-art frequency controllers at asset levels need to be incorporated in the power plant control architecture. In this paper, a novel hierarchical FC approach using FROB is proposed to allow the provision of a wide range of FCSs, specifically fast FCSs provided by asset controllers, for a HPP that consists of heterogeneous assets. To authors' knowledge, this paper is the first literature to date that discusses how to incorporate frequency responses provided by asset controllers in a hierarchical power plant control architecture. The main contribution of this approach is threefold: i) A new frequency control architecture is proposed to allow the provision of three types of FCSs including FFR, FCR and FRR. Controllers for fast FCSs
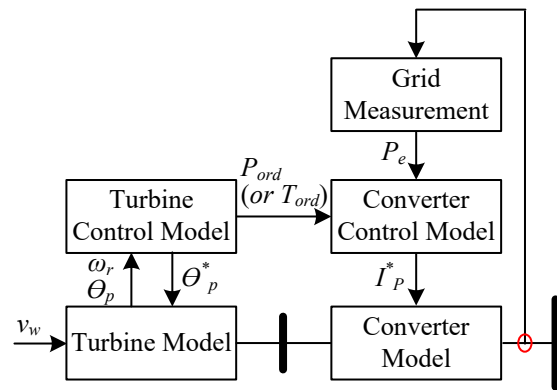

Fig. 2: WT dynamic model.

like FFR and FCR are implemented at asset controllers and controllers for slow FCS like FRR is implemented at plant controllers and the HPPC. It is demonstrated by simulation results that this frequency control architecture outperforms the state-of-the-art power plant control architecture, which is a centralized approach; ii) An innovative FROB is introduced at plant controllers and the HPPC to avoid control counteraction against asset controllers. Design guidelines on FROB are given; iii) Robustness analysis has been done to evaluate the performance of the proposed FROB when there are system uncertainties in the HPP. It is discovered that the FROB achieves robust performance against various types of uncertainties, including parameter uncertainty, unknown control malfunction, and time-varying communication delays.

Next section introduces dynamic modeling of HPPs with the proposed hierarchical FC approach. Section III starts with a brief introduction of the DOB and then focuses on FROB design and analysis. In Section IV, simulations are conducted and the effectiveness of the proposed control is illustrated. Section V concludes the paper.

II. DYNAMIC MODELING AND CONTROL OF HPP

A. HPP Component Model

The dynamic models for WTs, PVs and ESs are shown in Fig. 2, Fig. 3 and Fig. 4, respectively, along with converter models and converter control models. Since this paper is concerned with FC, only active power control module is considered in converter control. Reactive power control module is beyond the scope.

The WT dynamic model is built based on a variable speed Type 4 WT configuration [27]. Turbine model consists of a simplified aerodynamic model and a two-mass model used for representing the drive train of the WT. Turbine control model consists of two submodules, torque control and pitch angle control. Torque control is employed based on a two-dimensional aerodynamic torque coefficient table [28] while pitch angle control is developed according to IEC 61400-27-1 [29]. Converter control model and converter model are also described in [29].

The PV dynamic model is built based on a generic two-stage PV system model for large-scale SPPs. The PV panel module is represented using the standard single-diode model [30].
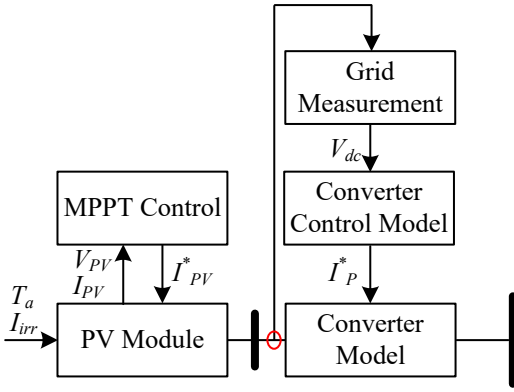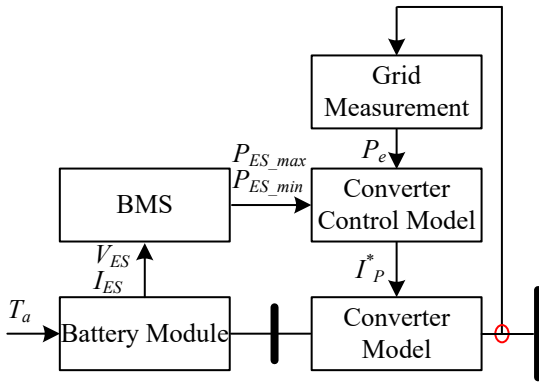
Fig. 3: PV dynamic model.

Fig. 4: ES dynamic model.

Maximum power point tracking (MPPT) controller seeks for maximum power point of the PV panel module given weather conditions, and PV terminal voltage and current. Converter control model and converter model are described in [31].

The ES dynamic model is built based on a generic ES model. The battery bank module comprising a voltage source in series with a resistor is considered based on [11], [32], [33]. The battery management system (BMS) has been developed in order to estimate state of charge and to determine maximum discharging and charging current for ES converter control model. The input of the BMS includes ES terminal voltage and current. Converter control model and converter model are described in [34].

B. Hierarchical Frequency Control

In the existing approaches, controllers for FFR and FCR are integrated into plant controllers via the auxiliary FC loop added to active power control [6], [10]. However, these approaches could lead to a degraded frequency response due to several factors, such as communication delay or failures, control bandwidth limit, and ramp rate limit. To make the speed of frequency response free from the restriction by the above-mentioned factors, a hierarchical FC architecture, consisting of three control levels, asset controllers, plant controllers and the HPPC, is proposed, as shown in Fig. 5. By having controllers for FFR and FCR implemented at asset controllers, FCSs are activated by local frequency measurement, and no

communication is required. Besides, control bandwidth of asset controllers is designed to be sufficiently large to support fast FC. Control signal for fast FC also bypasses the limit on the reference ramp rate.

It is also seen in Fig. 5 that the FROB is implemented within the plant controllers and the HPPC. These controllers, located in the plant control room, receive setpoints from HPP energy management system (EMS) and system operator. An extra loop of the FROB is added to active power measurement for the controllers to avoid control counteraction with asset controllers.

The references sent from the HPPC to plant controllers are defined as follows:

$$
\begin{aligned}
\boldsymbol{u_{WPP}} = &[P^*_{WPP}, \boldsymbol{P^*_{WPP+}}, \boldsymbol{P^*_{WPP-}}, \boldsymbol{T_{FFR}}, \\
&DB_{FFR}, DB_{FCR}, R_{FCR}]
\end{aligned}
\tag{1}
$$

$$
\begin{aligned}
\boldsymbol{u_{SPP}} = &[P^*_{SPP}, \boldsymbol{P^*_{SPP+}}, \boldsymbol{P^*_{SPP-}}, \boldsymbol{T_{FFR}}, \\
&DB_{FFR}, DB_{FCR}, R_{FCR}]
\end{aligned}
\tag{2}
$$

$$
\begin{aligned}
\boldsymbol{u_{ESS}} = &[P^*_{ESS}, \boldsymbol{P^*_{ESS+}}, \boldsymbol{P^*_{ESS-}}, \boldsymbol{T_{FFR}}, \\
&DB_{FFR}, DB_{FCR}, R_{FCR}]
\end{aligned}
\tag{3}
$$

where P^*_{WPP}, P^*_{SPP}, and P^*_{ESS} are power references for WPP, SPP and ESS, respectively. $\boldsymbol{P^*_{WPP+}}$, $\boldsymbol{P^*_{WPP-}}$, $\boldsymbol{P^*_{SPP+}}$, $\boldsymbol{P^*_{SPP-}}$, $\boldsymbol{P^*_{ESS+}}$ and $\boldsymbol{P^*_{ESS-}}$ are upwards and downwards frequency reserve vectors for WPP, SPP and ESS, respectively. Each frequency reserve vector contains three elements representing the amount of FFR, FCR and FRR, respectively. $\boldsymbol{T_{FFR}}$ is a time vector that defines rising time, duration and falling time of FFR. DB_{FFR}, DB_{FCR} and R_{FCR} are frequency deadband of FFR, frequency deadband and droop coefficients of FCR, respectively. The references sent from plant controllers to asset controllers are defined as follows:

$$
\begin{aligned}
\boldsymbol{u_{WTi}} = &[P^*_{WTi}, \boldsymbol{P^*_{WT+}}, \boldsymbol{P^*_{WT-}}, \boldsymbol{T_{FFR}}, \\
&DB_{FCR}, R_{FCR}]
\end{aligned}
\tag{4}
$$

$$
\begin{aligned}
\boldsymbol{u_{PVi}} = &[P^*_{PVi}, \boldsymbol{P^*_{PV+}}, \boldsymbol{P^*_{PV-}}, \boldsymbol{T_{FFR}}, \\
&DB_{FCR}, R_{FCR}]
\end{aligned}
\tag{5}
$$

$$
\begin{aligned}
\boldsymbol{u_{ESi}} = &[P^*_{ESi}, \boldsymbol{P^*_{ES+}}, \boldsymbol{P^*_{ES-}}, \boldsymbol{T_{FFR}}, \\
&DB_{FCR}, R_{FCR}]
\end{aligned}
\tag{6}
$$

where P^*_{WTi}, P^*_{PVi}, and P^*_{ESi} are power references for the ith WT, the ith PV and the ith ES, respectively. $\boldsymbol{P^*_{WT+}}$, $\boldsymbol{P^*_{WT-}}$, $\boldsymbol{P^*_{PV+}}$, $\boldsymbol{P^*_{PV-}}$, $\boldsymbol{P^*_{ES+}}$ and $\boldsymbol{P^*_{ES-}}$ are upwards and downwards frequency reserve vectors for the ith WT, the ith PV and the ith ES, respectively. $\boldsymbol{T_{FFR}}$, DB_{FFR}, DB_{FCR} and R_{FCR} are the same FC settings as the ones passed from the HPPC. Note that once fixed, these settings are rarely updated.

As shown in Fig. 6, a parallel control loop for FFR and FCR is implemented at asset controllers. Controller for FCR is implemented using a droop control with frequency deadband, while controller for FFR is implemented using an open-loop pre-defined shape with a FFR activation block. The output of this control loop is added to active power control of asset
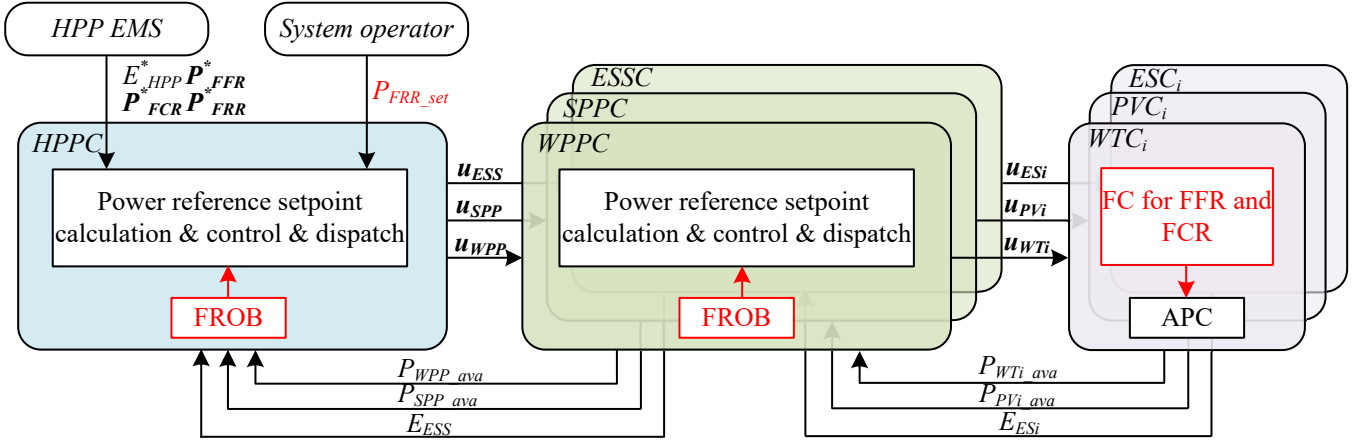
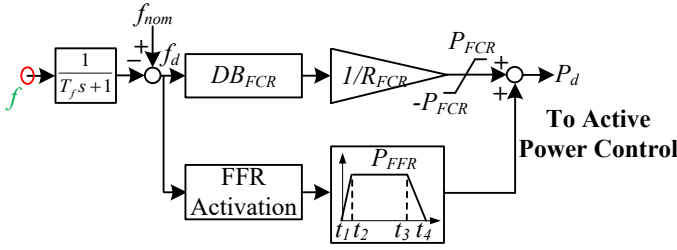Fig. 5: The proposed hierarchical FC architecture.
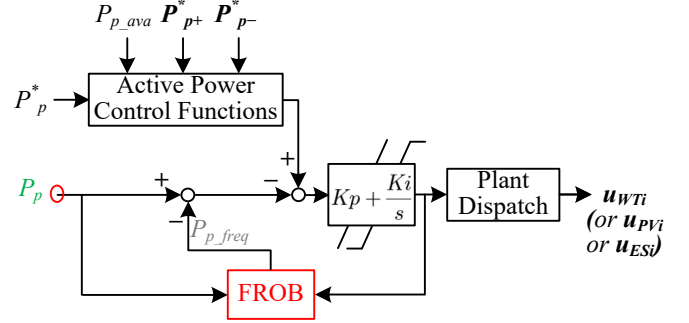

Fig. 6: Frequency controller for FFR and FCR.

Fig. 7: Plant controller design.

controllers [27]. It is worth pointing out that the proposed asset controller design is only an example and there are alternatives for implementing controllers for FFR and FCR with comparable performance [15]. To develop the optimal FC strategy from the assets is beyond the focus of the paper.

Fig. 7 shows the diagram of a plant controller, whose structure is universally applicable to the WPPC, the SPPC and the ESSC. While no FC is implemented at the plant controller, a FROB is added to estimate the total frequency response from asset controllers. By subtracting the FROB output from active power measurement at plant point of connection (PoC), the compensated feedback only contains active power measurement irrelevant to FC. Another FROB is also added to the HPPC for the same purpose, as shown in Fig. 8, allowing the HPPC to provide a stacked functionality of energy trade and FCS provision. Controller for FRR is implemented at the HPPC given that the response of FRR is slow, in the range of tens of minutes. An extra control setpoint P_{FRR_set} is added to HPP active power controller to control the activation of FRR. The design details of plant controller and the HPPC could be found in the companion paper [19].

III. FREQUENCY RESPONSE OBSERVER

The idea of FROB is inspired by frequency-domain DOBs which accurately track uncertainties and unknown disturbances. From the perspective of plant controllers and the HPPC, frequency responses activated at asset controllers can be considered as "unknown disturbances with uncertainties".
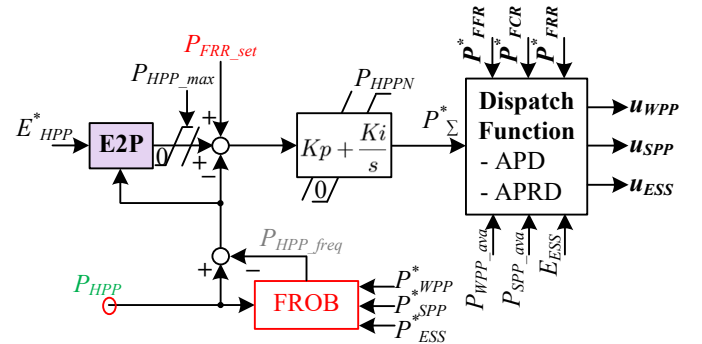

Fig. 8: The HPPC design.

The difference that distinguishes FROB from frequency-domain DOBs is that the total frequency response should be accepted rather than rejected at plant controllers and the HPPC. This section briefly reviews classical frequency-domain DOBs and then gives design guidelines and robustness analysis for FROB.

A. Overview of DOB

Frequency-domain DOBs were initially proposed in [26] to improve the robustness of the controllers for DC servo motor systems, given disturbances and uncertainties in the system. As shown in Fig. 9, the lumped disturbance $d_l(s)$ is written
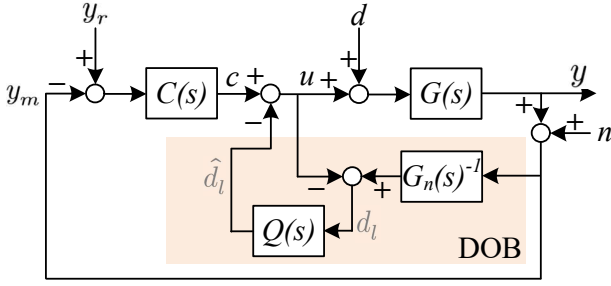
Fig. 9: A generic DOB structure.

Fig. 10: FROB design for plant controller.

Fig. 11: Linearized unity feedback system.

as [35]:

$$d_l(s) = [G_n(s)^{-1} - G(s)^{-1}]y(s) + d(s) + G_n(s)^{-1}n(s) \tag{7}$$

where $d_l(s)$ captures all the disturbance and the uncertainties in the system. $G(s)$ and $G_n(s)$ are the physical system and the nominal model, respectively. $y(s)$ is the system output. $d(s)$ is the external disturbance. $n(s)$ is the measurement noise. The filter $Q(s)$ is used to estimate the lumped disturbance. The estimated lump disturbance $\hat{d}_l(s)$ is given by:

$$\hat{d}_l(s) = Q(s)d_l(s) \tag{8}$$

As the estimated lump disturbance is fed back to compensate the influence of the disturbance, the output of the equivalent system considering the DOB is expressed as:

$$y(s) = G_{cy}(s)c(s) + G_{dy}(s)d(s) + G_{ny}(s)n(s) \tag{9}$$

where $G_{cy}(s)$, $G_{dy}(s)$ and $G_{ny}(s)$ are transfer functions from $c(s)$, $d(s)$ and $n(s)$ to $y(s)$, respectively. In the frequency range where $Q(s) \approx 1$, (9) reduces to [35]:

$$y(j\omega) \approx G_n(j\omega)c(j\omega) - n(j\omega) \tag{10}$$

The above representation implies the real physical system is forced to behave like the nominal system without disturbance given $Q(s) \approx 1$.

B. FROB

As shown in Fig. 9, the input of frequency-domain DOBs u and y_m are internal to the controller. Likewise, Fig. 10 shows that the signals FROB uses are internally from plant controllers. Therefore, no communication links are needed during FCS provision. The main difference between the FROB design and the original frequency-domain DOB design lies in where the output of the observer goes. The DOB design adds the estimated disturbance directly to the output of the controller $C(s)$, leading to the suppression of disturbance and uncertainty. Here in the proposed FROB design, the estimated disturbance is added to the input of the controller $C_p(s)$ in order to compensate the frequency response and avoid control counteraction.

Fig. 10 shows the generic diagram of FROB, which is applicable to WPPCs, SPPCs and ESSCs. Asset level includes controller before FC C_{A1}, controller after FC C_{A2}, asset dynamics G_A and asset FC G_d. The input of G_d is the
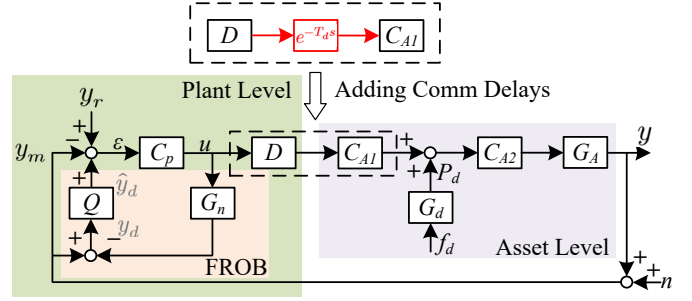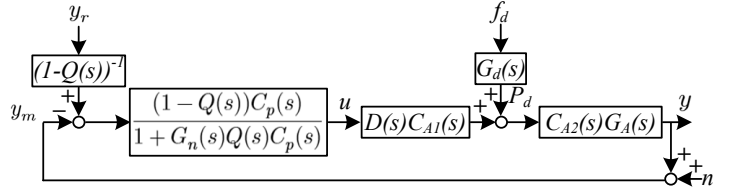
measured frequency deviation f_d and the output of G_d is the FC setpoint P_d. Output at asset level is the total power output y, and n represents measurement noise. Plant level includes plant controller C_p, dispatch function D, and the FROB. To implement FROB in plant controller, the nominal model G_n and the FROB filter Q should be obtained. G_n is the nominal representation of G, where $G = DC_{A1}C_{A2}G_A$, and can be derived in frequency domain based on benchmark models provided from manufacturers. The selection of Q will be covered later in Section III-C. The combined frequency response of FFR and FCR is estimated by taking the difference between y_m and $G_n u$. Ideally, it is desired that

$$\hat{y}_d = Q(y_m - G_n u) \approx y_d \approx P_d C_{A2} G_A \tag{11}$$

Based on Fig. 10, plant controller with FROB is restructured as a linearized unity feedback system, shown in Fig. 11. Plant controller with FROB is equivalent to controller $C_p(s)$ reshaped by $Q(s)$ and $G_n(s)$, with a prefilter $\frac{1}{1-Q(s)}$ added to control reference y_r. The transfer function from control reference to output $G_{y_r y}(s)$ is defined as (12). The transfer function from FC setpoint to output $G_{P_d y}(s)$ is defined as (13). The transfer function from measurement noise to output $G_{ny}(s)$ is defined as (14). When the filter $Q(s) \approx 1$, the transfer functions are simplified into:

$$G_{y_r y}|_{Q \approx 1} \approx \frac{C_p G}{1 + C_p G_n} \tag{15}$$

$$G_{P_d y}|_{Q \approx 1} \approx C_{A2} G_A \tag{16}$$

$$G_{ny}|_{Q \approx 1} \approx 0 \tag{17}$$

It is seen from (16) and (17) that, when $Q(s)$ is close to 1, frequency response is fully accepted in the closed-loop system, and measurement noise is completely attenuated. Although the unity might seem a perfect design for $Q(s)$ for the above reasons, it would lead to two issues. One is a zero loop transfer

$$G_{y_r y}(s) = \frac{C_p(s)G(s)}{1 + Q(s)C_p(s)G_n(s) - Q(s)C_p(s)G(s) + C_p(s)G(s)} \tag{12}$$

$$G_{P_d y}(s) = C_{A2}(s)G_A(s)\frac{1 + Q(s)C_p(s)G_n(s)}{1 + Q(s)C_p(s)G_n(s) - Q(s)C_p(s)G(s) + C_p(s)G(s)} \tag{13}$$

$$G_{ny}(s) = -\frac{(1 - Q(s))C_p(s)G(s)}{1 + Q(s)C_p(s)G_n(s) - Q(s)C_p(s)G(s) + C_p(s)G(s)} \tag{14}$$
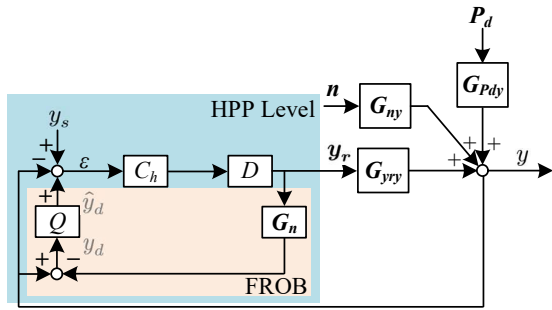

Fig. 12: FROB design for HPPC.

function, which causes difficulty in robustness analysis. The other is that the characteristics of reference setpoint tracking will be affected by the mismatch between G_n and G. Only when the nominal model is correct ($G_n = G$) does $G_{y_r y}(s)$ stay unchanged. Therefore, low-pass filters have been used for the design of $Q(s)$.

FROB for the HPPC is similar to FROB for plant controllers, as shown in Fig. 12. The difference lies mainly in the model being used in FROB to represent the nominal model of the HPP, $\boldsymbol{G_n}$, which is a multiple-input single-output model. The actual HPP dynamics are presented using the closed-loop transfer functions including both plant level and asset level. These closed-loop transfer functions for WPPs, SPPs and ESSs are obtained using (12), (13) and (14). A similar linearized unity feedback system to Fig. 11 can be easily derived including HPP level, plant level and asset level. To avoid redundancy, only plant level and asset level are considered as the example in the following design guideline and robustness analysis. Nevertheless, they can readily be applied to the system including all three levels.

C. Design Guidelines

The design of the filter $Q(s)$ plays a significant role in the FROB. The main requirement is that $Q(s)$ should be a low-pass filter with unity gain for low frequency to accept frequency response and zero gain for high frequency to attenuate measurement noise. Unlike the DOB filter design [36], [37], no degree requirements exist for the FROB filter since there is no inverse of the model. There is an amount of freedom to select $Q(s)$ as long as $Q(j\omega) \approx 1$ in the frequency range covering frequency response and measurement noise. The main parameters to be selected for $Q(s)$ are the cut-off frequency ω_c and the filter degree n. A straightforward

Algorithm 1 $Q(s)$ **Selection**

1: Initialize the algorithm by setting up a general structure for $Q(s)$:
$Q(s) = \frac{1 + \sum_{m=1}^{n-1} f_m s^m}{1 + \sum_{m=1}^{n} f_m s^m}$
2: Start the filter degree $n = 1$ and choose ω_c to be equal to or larger than the frequency of measurement noises.
3: Perform bode analysis of $G_{P_d y}$ and G_{ny}, and fine tune ω_c, such that $G_{P_d y}$ has unity gain around the frequency range of frequency response and G_{ny} has small gain around the frequency range of measurement noises.
4: Increase the filter degree by 1 and choose the butterworth filter coefficients while keeping the same ω_c. Check if $G_{P_d y}$ has unity gain for a wider frequency range, that is, a preferable performance on frequency response acceptance, and G_{ny} has a smaller gain for a wider frequency range, that is, a preferable performance on measurement noise attenuation.
5: **If** $G_{P_d y}$ and G_{ny} show a better performance with the increased filter degree
6:     **Repeat** Step 4.
7: **Else**
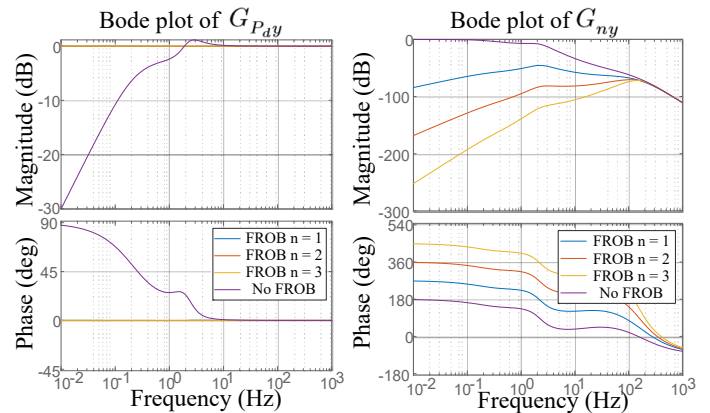8:   Finalize the design of $Q(s)$ with the original degree.

Fig. 13: Bode plots of transfer functions - $G_{P_d y}$ and G_{ny}.

algorithm is developed to select the filter $Q(s)$, shown as Algorithm 1.

Fig. 13 presents bode plots of $G_{P_d y}(s)$ and $G_{ny}(s)$. Without FROB being included, $G_{P_d y}(s)$ shows the rejection of frequency response in low frequency range, which explains the reason for control counteraction in hierarchical FC. With FROB being included, $G_{P_d y}(s)$ shows the characteristics of frequency response acceptance and stays unchanged as the filter degree increases. It is also seen that without FROB, $G_{ny}(s)$ shows a limited performance of measurement noise attenuation in low and medium frequency range. With a higher filter degree, the performance of measurement noise attenuation has been improved. Therefore, the degree of 3 is preferable for the design of $Q(s)$.

This article has been accepted for publication in IEEE Transactions on Sustainable Energy. This is the author's version which has not been fully edited and content may change prior to final publication. Citation information: DOI 10.1109/TSTE.2022.3217355

7

PI gains of plant controllers are selected with the consideration of performance requirements of reference setpoint tracking and coordination with other control levels. The bandwidth of the closed-loop system including plant level and asset level is selected to be 0.25 Hz and the phase margin is selected to be $150°$.

D. Robustness Analysis

In this subsection, robustness analysis under two scenarios are considered for the FROB: robustness in the presence of uncertain parameters and time-varying communication delay. When uncertainties are considered, it implies that $G_n(s) = G(s)$ is invalid.

In the first scenario, assume that asset dynamics has changed to a different system G'_A, leading to the actual physical system G_{m1} different from G_n, which is written as:

$$G_{m1} = DC_{A1}C_{A2}G'_A \qquad (18)$$

In the second scenario, time-varying communication delay is introduced between asset controllers and plant controllers as $e^{-T_d s}$ as shown in Fig. 10, and T_d is uncertain but is known to lie in the range $[T_1, T_2]$. Communication delay leads to another physical system G_{m2}, which is written as:

$$G_{m2} = e^{-T_d s}G = e^{-T_d s}DC_{A1}C_{A2}G_A \qquad (19)$$

Based on the perturbation multiplicative model [38], the magnitude bound for system stability in these two scenarios is written as:

$$M_1(s) = \frac{G'_A(s)}{G_A(s)} - 1 \qquad (20)$$

$$M_2(s) = e^{-T_d s} - 1 \qquad (21)$$

The loop transfer function of the FROB including an asset controller and a plant controller is derived from Fig. 11:

$$L(s) = \frac{(1 - Q(s))C_p(s)G(s)}{1 + Q(s)G_n(s)C_p(s)} \qquad (22)$$

To check the stability of the closed-loop system in the presence of uncertain parameters, it should be guaranteed that

$$|M_1(j\omega)| < |1 + \frac{1}{L(j\omega)}| \text{ for all } \omega \text{ and } a_{min} \le a \le a_{max} \qquad (23)$$

$$|M_2(j\omega)| < |1 + \frac{1}{L(j\omega)}| \text{ for all } \omega \text{ and } T_1 \le T_d \le T_2 \quad (24)$$

Since a and T are uncertain, the magnitude of the LHS of (23) and (24) are not known. As long as functions $W_1(s)$ and $W_2(s)$ are found, such that

$$|\frac{G'_A(j\omega)}{G_A(j\omega)} - 1| < |W_1(j\omega)| \text{ for all } \omega \text{ and } a_{min} \le a \le a_{max} \qquad (25)$$

$$|e^{-j\omega T_d} - 1| < |W_2(j\omega)| \text{ for all } \omega \text{ and } T_1 \le T_d \le T_2 \qquad (26)$$
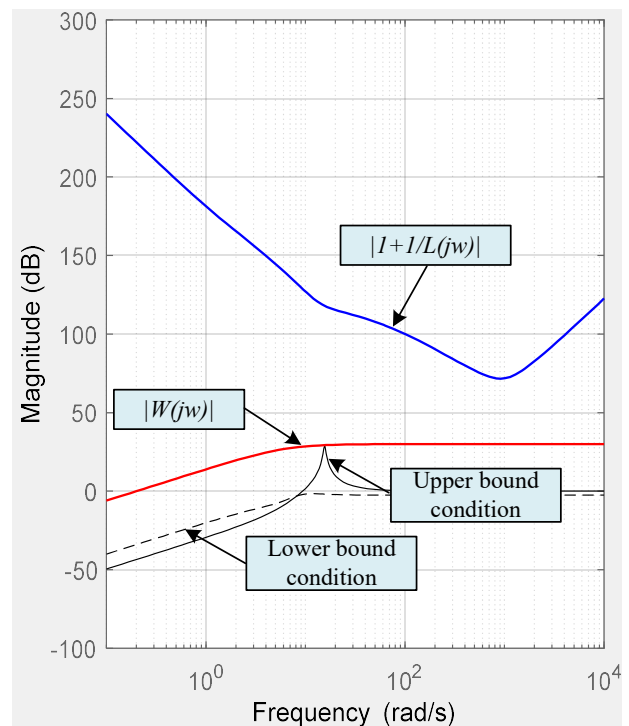

Fig. 14: Magnitude plot of $|M_1(j\omega)|$, $|W(j\omega)|$ and $|1 + \frac{1}{L(j\omega)}|$.

the robust stability conditions with uncertain parameters and time-varying communication delay are satisfied by

$$|W_1(j\omega)| < |1 + \frac{1}{L(j\omega)}| \text{ for all } \omega \qquad (27)$$

$$|W_2(j\omega)| < |1 + \frac{1}{L(j\omega)}| \text{ for all } \omega \qquad (28)$$

Fig. 14 and Fig. 15 shows magnitude plots for $|M(j\omega)|$, $|W(j\omega)|$ and $|1 + \frac{1}{L(j\omega)}|$ with two types of uncertainties. In Fig. 14, it can be seen that, when the actual dynamics vary around the nominal model, a function $W_1(s)$ can be obtained as the upper bound of $|\frac{G'_A(j\omega)}{G_A(j\omega)} - 1|$. Likewise, consider communication delay between plant controllers and asset controllers ranges from 0 to 2 sec for a large renewable power plant [39]. The function $W_2(s)$ is obtained as the upper bound of $|e^{-j\omega T_d} - 1|$. It is seen in Fig. 15 that the robust stability condition is met for both scenarios. Also a high magnitude of $|1 + \frac{1}{L(j\omega)}|$ indicates the FROB results in a very robust system.

IV. SIMULATION RESULTS

In order to validate the proposed hierarchical FC approach as well as the relevant analytical results, three case studies are carried out using a single-bus power system model with system parameters shown in [40]. This power system model, along with a detailed HPP model including the WPP, the SPP and the ESS and the corresponding controls, is built in MATLAB/Simulink™. Frequency control parameters, as shown in Table I, are chosen to comply with grid codes and technical requirements [41], [42]. The first case study is the
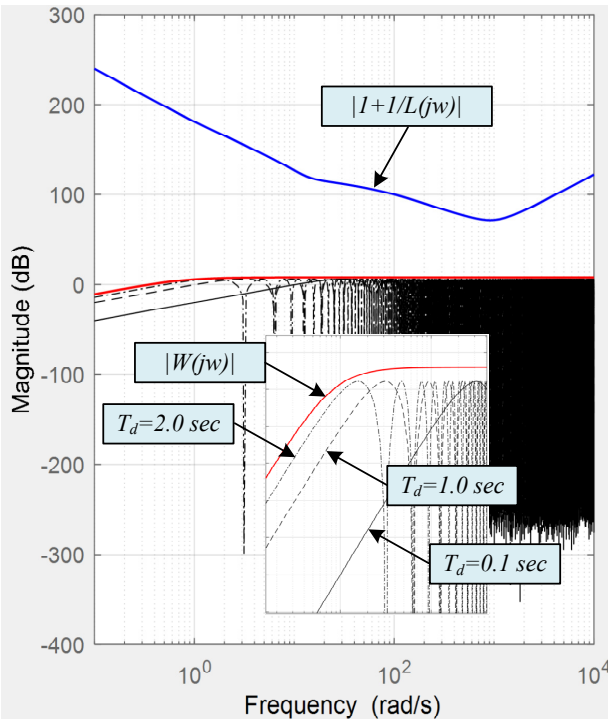
This article has been accepted for publication in IEEE Transactions on Sustainable Energy. This is the author's version which has not been fully edited and content may change prior to final publication. Citation information: DOI 10.1109/TSTE.2022.3217355

8

Fig. 15: Magnitude plot of $|M_2(j\omega)|$, $|W(j\omega)|$ and $|1+\frac{1}{L(j\omega)}|$.

TABLE I: Frequency Controller Parameters

FFR controller	
Deadband DB_{FFR} (Hz)	±0.3
Activation level (Hz)	49.7
Activation time (sec)	1.3
Support duration (sec)	5
FCR controller	
Deadband DB_{FCR} (Hz)	±0.1
Activation level (Hz)	49.9
Droop coefficient R_{FCR} (p.u.)	0.05
FRR controller	
Activation time (sec)	≥300

benchmark case showing the performance of the proposed FC on the coordination of three types of FCSs. The comparison with the centralized implementation is presented in the second case study. The focus of the third case study is on the robustness of the FROB when different types of uncertainties are included in the system.

A. Benchmark Studies

Fig. 16 shows frequency response provided by the HPP while the HPP tracks power setpoint decided by the HPP EMS. The under-frequency event is triggered at t = 150 sec by a heavy load switching-in within the power system. A secondary FC is initiated by system operator at t = 400 sec. Fig. 16a presents the case when all the FCSs including FFR, FCR and FRR are fulfilled by the ESS. At t = 150 sec when frequency dip occurs, the ESS provides a combined frequency response of FFR and FCR. After system frequency reaches a new steady-state, the charging power of the ESS achieves a new steady-state value, since FCR is still activated. At t = 400 sec, the FRR setpoint is sent to the HPPC by system operator,

and the frequency is restored back to 50 Hz by system-level secondary frequency response. Meanwhile, FCR deactivates as frequency deviation reduces to zero.

Fig. 16b presents another case when FCSs are fulfilled by both the ESS and the WPP. According to the active power reserve dispatch algorithm in [19], the capacity of the ESS is reserved to provide FFR and FCR, and the WPP runs at the derated operation to provide FCR and FRR. When the frequency dip occurs at t = 150 sec, the ESS provides a combined frequency response of FFR and FCR while the WPP provides FCR. At t = 400 sec, the FCR deactivates due to frequency restoration, and the charging power of the ESS returns to the pre-event value. Meanwhile, the WPP participates in secondary frequency response initiated by system operator via the contribution of FRR.

The above results show that the proposed hierarchical FC is effective in coordinating three types of FCSs, namely FFR, FCR and FRR, during frequency events. Besides, this approach allows stacked operation of FC and power reference tracking. Thanks to FROB, no counteraction is identified. More thorough operating scenarios will be considered as future work to validate the proposed approach.
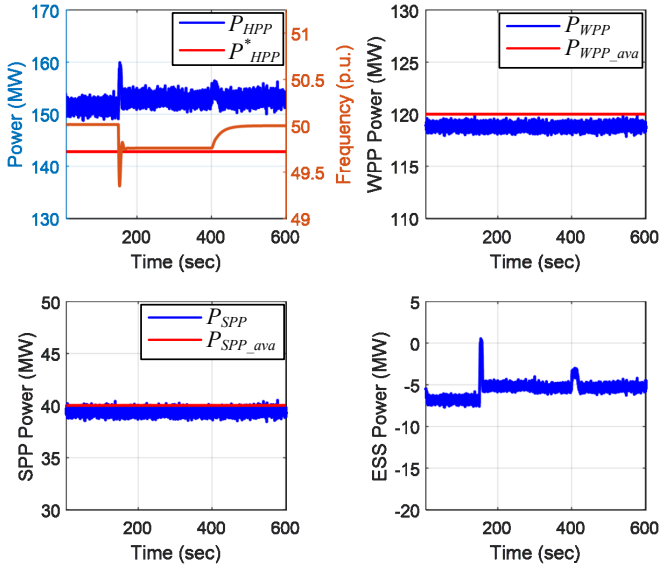
B. Comparison with Centralized Approach

In the existing work [6], FC has been implemented at the HPPC. Fig. 17 shows a simplified diagram for centralized implementation of FC. The main difference from the proposed approach is that the controller for FFR and the FCR is located at the HPPC and activated by the frequency measured at the HPP PoC. FC is enabled via active power control from the HPPC, of which active power setpoint is passed to active power control of each plant controller. Note that FROB is still needed at the HPPC to distinguish frequency response from active power tracking, but is unnecessary at plant controllers.

Fig. 18 presents a comparison between the proposed approach and the centralized approach in terms of the performance of FFR and FCR provision. The communication delay T_d is assumed to exist between asset controllers and plant controllers and to lie in the interval between 0 sec and 2 sec. Four values are selected: 0.0 sec, 0.1 sec, 1.0 sec and 2.0 sec. It is seen in Table II that with no or small communication delay, frequency response via the proposed approach and the centralized approach are comparable. However, for larger communication delay like 1 sec or 2 sec, the centralized approach provides a delayed frequency response that doesn't meet technical requirement of FFR and FCR [41], [42]. On the contrary, the proposed approach provides the same level of frequency response regardless of the communication delay. It is interesting to note that even if there is negligible communication delay, time constant of frequency response via the centralized approach is still larger than the proposed approach. It is because limited control bandwidth of plant controllers slows down frequency response in the centralized approach.

C. Study on FROB Robustness

In order to investigate the robustness of FROB, three types of uncertainties are considered in this subsection. The first

This article has been accepted for publication in IEEE Transactions on Sustainable Energy. This is the author's version which has not been fully edited and content may change prior to final publication. Citation information: DOI 10.1109/TSTE.2022.3217355

9

(a) Only ESS participates in FCS provision with HPP power reference equal to 0.9 p.u. and HPP power reserve reference equal to 0.05 p.u.
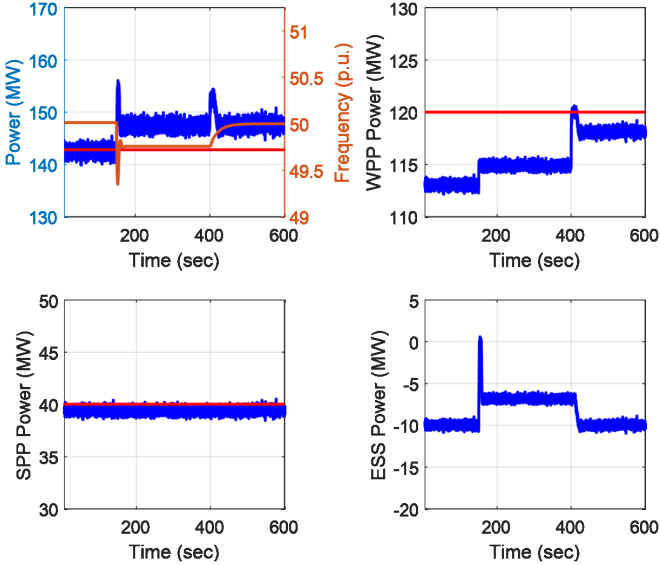
(b) Both WPP and ESS participate in FCS provision with HPP power reference equal to 0.84 p.u. and HPP power reserve reference equal to 0.10 p.u.

Fig. 16: FCS provision of an HPP during an under-frequency event.

type is uncertainty in system parameters. The second type is a random malfunction, which is unknown to the plant controller, of FC at asset level. The third type refers to time-varying communication delay between asset controllers and plant controllers. Either type of uncertainty leads to a nominal model $G_n(s)$ that doesn't represent the actual system $G(s)$. For simplicity purpose, only asset controllers and plant controllers are included in this study. However, the conclusion also applies to the case when the HPPC is considered.

To evaluate the performance of FROB, ideal responses of FFR and FCR are defined by the performance obtained from an open-loop plant controller. When the plant controller is
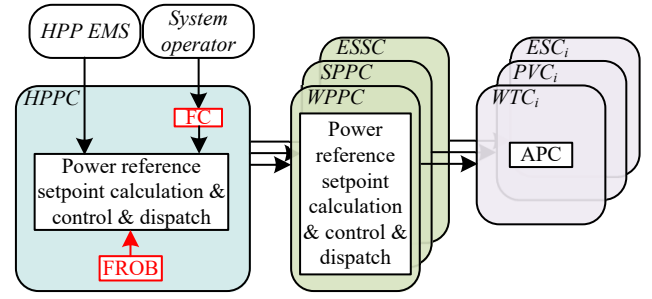

Fig. 17: Centralized implementation of hierarchical FC.

(a) $T_d = 0.0$ sec.   (b) $T_d = 0.1$ sec.
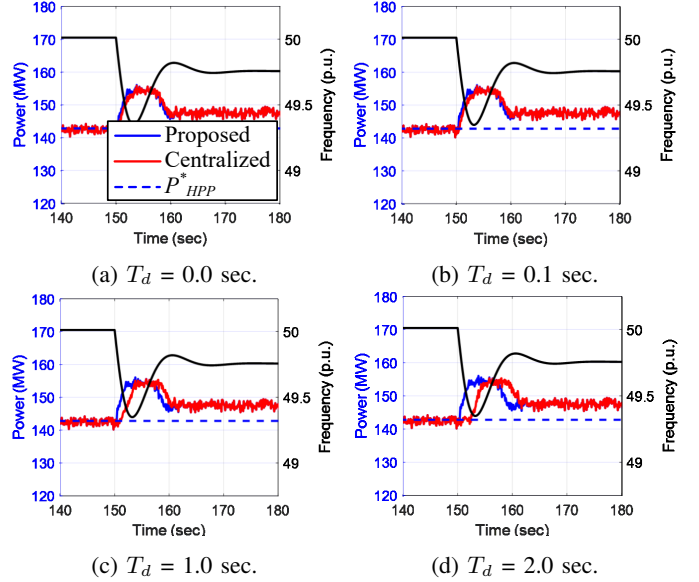
(c) $T_d = 1.0$ sec.   (d) $T_d = 2.0$ sec.

Fig. 18: Performance comparison of FCS provision between the proposed approach and the centralized approach considering communication delay.

open-loop, there is no counteraction between asset controllers and plant controllers during the frequency event. Another coordination strategy to avoid counteraction is to estimate the total frequency response from asset controllers using FC settings that are made available to plant controllers, plus the frequency measured at the plant PoC. In the following studies, the above-mentioned strategies are named Strategy #1 and Strategy #2, respectively. The proposed approach is named Strategy #3.

1) Impact of uncertain system parameters: The HPP might have several parameters that are constants but uncertain within a range. When actual parameters deviate from the nominal values used in the FROB design, the performance of FROB should be investigated. For example, control parameters of an asset converter vary around a nominal value that is used to construct the nominal WPP model for the FROB. Here, uncertainties in parameters are considered as:

$$\delta 1 = T_{cc\_MSC} \in [0.001, 0.1], \delta 2 = K_{p\_pc\_MSC} \in [0.05, 0.15],$$
$$\delta 3 = K_{i\_pc\_MSC} \in [5, 15], \delta 4 = T_{cc\_GSC} \in [0.001, 0.1],$$
$$\delta 5 = K_{p\_vc\_GSC} \in [7.5, 22.5], \delta 6 = K_{i\_vc\_GSC} \in [75, 225].$$
$$(29)$$

TABLE II: Impact of Communication Delay on Frequency Response Provision

Comm Delay T_d (sec)	Rise Time (sec)	
	Distributed	Centralized
0.0	1.9	2.9
0.1	1.9	2.9
1.0	1.9	3.4
2.0	1.9	4.6
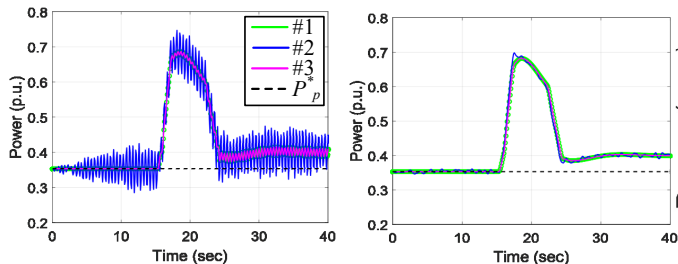
(a) upper bound uncertainties.   (b) lower bound uncertainties.

Fig. 19: FROB robustness considering uncertain system parameters.

where T_{cc_MSC} is time constant of current control of machine-side converter, $K_{p\_pc\_MSC}$ and $K_{i\_pc\_MSC}$ are proportional and integral gains of power control of machine-side converter, T_{cc_GSC} is time constant of current control of grid-side converter, $K_{p\_vc\_GSC}$ and $K_{i\_vc\_GSC}$ are proportional and integral gains of DC-link voltage control of grid-side converter. Fig. 19a and 19b shows frequency responses for upper and lower bound uncertain systems. Strategy #3 always provides frequency response identical to the ideal response (Strategy #1). On the other hand, the deviation of system parameters causes the failure of estimating frequency responses from asset controllers using Strategy #2. Thus, FROB shows robustness over uncertain systems.

2) Impact of unknown FC malfunction: It happens when FC at some assets fail to respond to frequency dips due to device malfunction. When the failure is unknown to plant controller, whether frequency response is properly coordinated across control hierarchy needs to be investigated. Fig. 20 shows that frequency response from Strategy #3 adaptively coincides with that from Strategy #1. It implies that FROB is robust in estimating the total frequency response, regardless of what percentage of assets experience FC failure. Meanwhile, frequency response from Strategy #2 indicates that the total frequency response from all the assets is overestimated by plant controller because plant controller has not been notified of those malfunctioning units.

3) Impact of time-varying communication delay: The exact value of communication delay between asset controllers and plant controllers is uncertain, and the interval $0 \leq T_d \leq 2s$ is used. Fig. 21 shows frequency response considering T_d equal to 0.0 sec, 0.1 sec, 1.0 sec and 2.0 sec. While Strategy #2 experiences instability issues with large communication delay, there is no stability issue observed from Strategy #3, which in all cases provides the identical frequency response to that of Strategy #1. Although tuning control gains could be an
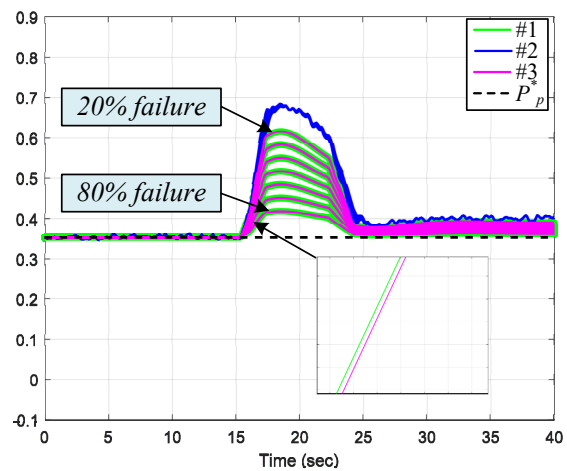

Fig. 20: FROB robustness considering unknown FC malfunction.

(a) T_d = 0.0 sec.   (b) T_d = 0.1 sec.

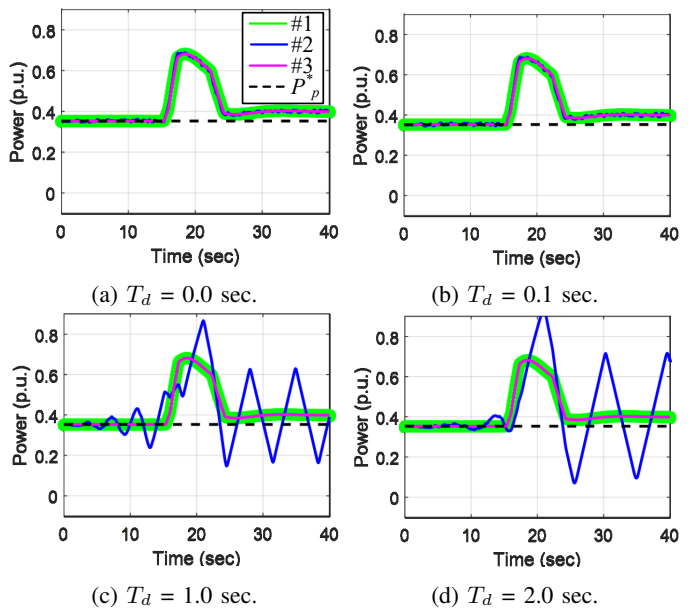(c) T_d = 1.0 sec.   (d) T_d = 2.0 sec.

Fig. 21: FROB robustness considering time-varying communication delay.

option of resolving instability for Strategy #2, it could still be challenging to obtain a set of control gains accommodating time-varying communication delay. With the FROB integrated into plant controllers, control gains can be kept the same as those designed for cases without communication latency. This characteristic shows the superior performance of the FROB regarding robustness against time-varying communication delay.

V. CONCLUSION

This paper proposes an innovative hierarchical FC approach that enables HPPs to provide FCSs. The proposed approach coordinates not only among multiple technology power plants but also across control hierarchy. Fast FCSs like FFR and FCR are implemented at asset level while slow FCS such as FRR is implmented at plant level and HPP level. A novel observer

called FROB, which is inspired by frequency-domain DOBs, is developed to estimate the total frequency responses activated by asset controllers, for the purpose of avoiding control counteraction. In this way, the proposed approach accommodates state-of-the-art fast FC designed at asset level, coping with the increasingly demanding technical requirements. From the case studies performed, it is evident that the proposed hierarchical FC approach using FROB provides coordinated FCSs even when there are system uncertainties, such as uncertain control parameters, unknown malfunction or time-varying communication delay. Application of the proposed hierarchical FC approach in power plants adopting other inverter-based or synchronous generation technology are under further research and development.

ACKNOWLEDGMENT

REFERENCES

[1] R. Eriksson, N. Modig, and M. Kuivaniemi, "Ensuring future frequency stability in the Nordic Synchronous Area," in *18th International Wind Integration Workshop*, Dublin, Ireland, 2019, pp. 1–7.

[2] W. Gorman, A. Mills, M. Bolinger, R. Wiser, N. G. Singhal, E. Ela, and E. O'Shaughnessy, "Motivations and options for deploying hybrid generator-plus-battery projects within the bulk power system," *Electricity Journal*, vol. 33, no. 5, p. 106739, 2020. [Online]. Available: https://doi.org/10.1016/j.tej.2020.106739

[3] WindEurope, "Renewable Hybrid Power Plants - Exploring the benefits and market opportunities," Tech. Rep., 2019.

[4] WindEurope, "Database for wind + storage co-located projects," [Online]. Available: https://windeurope.org/about-wind/database-for-wind-and-storage-colocated-projects/.

[5] K. Das, A. D. Hansen, M. Koivisto, and P. E. Sørensen, "Enhanced features of wind-based hybrid power plants," in *4th International Hybrid Power Systems Workshop*, Crete, Greece, 2019, pp. 22–23.

[6] D. V. Pombo, F. Iov, and D. I. Stroe, "A novel control architecture for hybrid power plants to provide coordinated frequency reserves," *Energies*, vol. 12, no. 5, 2019.

[7] Q. Long, A. Celna, K. Das, and P. Sørensen, "Fast frequency support from hybrid wind power plants using supercapacitors," *Energies*, vol. 14, no. 12, 2021.

[8] A. D. Hansen, P. Sørensen, F. Iov, and F. Blaabjerg, "Centralised power control of wind farm with doubly fed induction generators," *Renewable Energy*, vol. 31, no. 7, pp. 935–951, 2006.

[9] B. R. Karthikeya and R. J. Schutt, "Overview of wind park control strategies," *IEEE Transactions on Sustainable Energy*, vol. 5, no. 2, pp. 416–422, 2014.

[10] R. K. Varma and M. Akbari, "Simultaneous fast frequency control and power oscillation damping by utilizing PV solar system as PV-STATCOM," *IEEE Transactions on Sustainable Energy*, vol. 11, no. 1, pp. 415–425, 2020.

[11] F. Calero, C. A. Canizares, and K. Bhattacharya, "Dynamic modeling of battery energy storage and applications in transmission systems," *IEEE Transactions on Smart Grid*, vol. 12, no. 1, pp. 589–598, 2021.

[12] S. I. Nanou, A. G. Papakonstantinou, and S. A. Papathanassiou, "A generic model of two-stage grid-connected PV systems with primary frequency response and inertia emulation," *Electric Power Systems Research*, vol. 127, pp. 186–196, 2015. [Online]. Available: http://dx.doi.org/10.1016/j.epsr.2015.06.011

[13] H. Xin, Y. Liu, Z. Wang, D. Gan, and T. Yang, "A new frequency regulation strategy for photovoltaic systems without energy storage," *IEEE Transactions on Sustainable Energy*, vol. 4, no. 4, pp. 985–993, 2013.

[14] A. F. Hoke, M. Shirazi, S. Chakraborty, E. Muljadi, and D. Maksimovic, "Rapid active power control of photovoltaic systems for grid frequency support," *IEEE Journal of Emerging and Selected Topics in Power Electronics*, vol. 5, no. 3, pp. 1154–1163, 2017.

[15] Z. Wu, W. Gao, T. Gao, W. Yan, H. Zhang, S. Yan, and X. Wang, "State-of-the-art review on frequency response of wind power plants in power systems," *Journal of Modern Power Systems and Clean Energy*, vol. 6, no. 1, pp. 1–16, 2018.

[16] J. Licari, J. Ekanayake, and I. Moore, "Inertia response from full-power converter-based permanent magnet wind generators," *Journal of Modern Power Systems and Clean Energy*, vol. 1, no. 1, pp. 26–33, 2013.

[17] Y. Liu, J. R. Gracia, T. J. King, and Y. Liu, "Frequency regulation and oscillation damping contributions of variable-speed wind generators in the U.S. Eastern Interconnection (EI)," *IEEE Transactions on Sustainable Energy*, vol. 6, no. 3, pp. 951–958, 2015.

[18] H. Wang, Z. Chen, and Q. Jiang, "Control method for variable speed wind turbines to support temporary primary frequency control," in *Proceedings of the IEEE Power Engineering Society Transmission and Distribution Conference*, no. 1. IEEE, 2014, pp. 1–5.

[19] Q. Long, K. Das, D. V. Pombo and P. E. Sørensen, "Hierarchical control architecture of co-located hybrid power plants," *International Journal of Electrical Power & Energy Systems*, vol. 143, 2022.

[20] E. A. Khousa and A. Ismail, "Active disturbance rejection control - based load frequency controller of interconnected power systems involving wind power penetration," in *2013 7th IEEE GCC Conference and Exhibition, GCC 2013*. IEEE, 2013, pp. 401–406.

[21] F. Liu, Y. Li, Y. Cao, J. She, and M. Wu, "A two-layer active disturbance rejection controller design for load frequency control of interconnected power system," *IEEE Transactions on Power Systems*, vol. 31, no. 4, pp. 3320–3321, 2016.

[22] X. Chang, Y. Li, W. Zhang, N. Wang, and W. Xue, "Active disturbance rejection control for a flywheel energy storage system," *IEEE Transactions on Industrial Electronics*, vol. 62, no. 2, pp. 991–1001, 2015.

[23] S. Saxena and Y. V. Hote, "Load frequency control in power systems via internal model control scheme and model-order reduction," *IEEE Transactions on Power Systems*, vol. 28, no. 3, pp. 2749–2757, 2013.

[24] M. Elkayam, S. Kolesnik, and A. Kuperman, "Guidelines to classical frequency-domain disturbance observer redesign for enhanced rejection of periodic uncertainties and disturbances," *IEEE Transactions on Power Electronics*, vol. 34, no. 4, pp. 3986–3995, 2019.

[25] M. Sitbon, S. Schacham, and A. Kuperman, "Disturbance observer-based voltage regulation of current-mode-boost-converter-interfaced photovoltaic generator," *IEEE Transactions on Industrial Electronics*, vol. 62, no. 9, pp. 5776–5785, 2015.

[26] K. Ohishi, M. Nakao, K. Ohnishi, and K. Miyachi, "Microprocessor-controlled DC motor for load-insensitive position servo system," *IEEE Transactions on Industrial Electronics*, vol. IE-34, no. 1, pp. 44–49, 1987.

[27] I. D. Margaris, S. A. Papathanassiou, N. D. Hatziargyriou, A. D. Hansen, and P. Sorensen, "Frequency control in autonomous power systems with high wind power penetration," *IEEE Transactions on Sustainable Energy*, vol. 3, no. 2, pp. 189–199, 2012.

[28] A. D. Hansen and G. Michalke, "Fault ride-through capability of DFIG wind turbines," *Renewable Energy*, vol. 32, no. 9, pp. 1594–1610, 2007.

[29] IEC, "Wind energy generation systems - Part 27-1: Electrical simulation models - Generic models," Genova, Switzerland, p. 94, 2015.

[30] V. D. Paduani, H. Yu, B. Xu, and N. Lu, "A unified power-setpoint tracking algorithm for utility-scale PV systems with power reserves and fast frequency response capabilities," *IEEE Transactions on Sustainable Energy*, vol. 13, no. 1, 2022.

[31] WECC Modeling and Validation Work Group, "Solar photovoltaic power plant modeling and validation guideline," WECC, Tech. Rep., 2019.

[32] F. Xie, H. Yu, Q. Long, W. Zeng and N. Lu, "Battery model parameterization using manufacturer datasheet and field measurement for real-time HIL applications," *IEEE Transactions on Smart Grid*, vol. 11, no. 3, pp. 2396–2406, 2020.

[33] Á. Ortega and F. Milano, "Generalized model of VSC-based energy storage systems for transient stability analysis," *IEEE Transactions on Power Systems*, vol. 31, no. 5, pp. 3369–3380, 2016.

[34] WECC Modeling and Validation Work Group, "WECC battery storage dynamic modeling guideline," WECC, Salt Lake City, Tech. Rep., 2016.

[35] W. H. Chen, J. Yang, L. Guo, and S. Li, "Disturbance-observer-based control and related methods - an overview," *IEEE Transactions on Industrial Electronics*, vol. 63, no. 2, pp. 1083–1095, 2016.

[36] T. Umeno, T. Kaneko, and Y. Hori, "Robust servosystem design with two degrees of freedom and its application to novel motion control of robot manipulators," *IEEE Transactions on Industrial Electronics*, vol. 40, no. 5, 1993.

[37] E. Schrijver and J. Van Dijk, "Disturbance observers for rigid mechanical systems: Equivalence, stability, and design," *Journal of Dynamic Systems, Measurement and Control, Transactions of the ASME*, vol. 124, no. 4, pp. 539–548, 2002.

[38] J. C. Doyle, A. B. Francis, and A. Tannenbaum, *Feeback control theory*. New York: Macmillan, 1992.

[39] X. Shi, Y. Cao, M. Shahidehpour, Y. Li, X. Wu, and Z. Li, "Data-driven wide-area model-free adaptive damping control with communication delays for wind farm," *IEEE Transactions on Smart Grid*, vol. 11, no. 6, 2020.

[40] K. Das, "Integration of renewable generation in power system defence plans," Ph.D. dissertation, Technical University of Denmark, 2016.

[41] ENTSO-E, "Technical Requirements for Frequency Containment Reserve Provision in the Nordic Synchronous Area," Brussels, Belgium, p. 38, 2021.

[42] ENTSO-E, "Technical Requirements for Fast Frequency Reserve Provision in the Nordic Synchronous Area," Brussels, Belgium, p. 17, 2021.
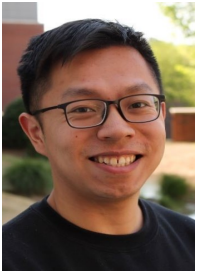
Qian Long (Member, IEEE) received the B.S. degree in electrical engineering from China Agricultural University, Beijing, China, in 2014, and both the M.S. degree and the Ph.D. degree in electrical engineering from North Carolina State University, Raleigh, NC, USA, in 2016 and 2020, respectively. He is currently a Senior Power System Design Engineer with ABB AS in Oslo, Norway. From 2020 to 2022, He was a Postdoctoral Researcher with Technical University of Denmark. His research interests are in the areas of modeling, operation, control and optimization of hybrid energy systems.

Kaushik Das (Senior Member, IEEE) received his Ph.D. degree from the Technical University of Denmark (DTU) in 2016. He is currently a Senior Researcher with DTU Wind Energy. His research interests include hybrid power and energy plants, power system balancing and grid integration of renewables in power systems. He is a member of IEA Wind, CIGRE, and other professional bodies. He is operating agent for IEA Wind Task 50 on Hybrid Wind Power Plants. He received the prestigious AEG Elektronfonden's Elektron Award in 2022.

Poul Sørensen (Fellow, IEEE) was born in 1958. He received the M.Sc. degree in electrical engineering from Technical University of Denmark (DTU), Denmark, in 1987. He is currently a Professor in wind power integration and control with the Department of Wind Energy, Technical University of Denmark, Denmark. He is Convener of IEC 61400-27 electrical simulation models for wind power generation. He is also Principal Investigator and Work Package leader in several research projects and has supervised 20 Ph.D. students and 30 Master's thesis. He was the Editor of Wiley Wind Energy 2007–2013. He has been IEEE Senior Member since 2007, and he became IEEE Fellow Member in 2021 for his contributions to wind power converter control and grid integration.